Design and Optimisation of High-Energy Inverse Compton Scattering Sources Driven By Multi-Pass Energy Recovery Linacs

Joe Crone
2nd Year Progression Report
Supervised by Dr H. Owen & Dr B. Muratori
The Cockcroft Institute & University of Manchester, Faculty of Science & Engineering

June 30, 2020

Preface: Covid-19

Covid-19 has disrupted work toward this PhD, however this was minimal. The long term attachment at Cornell University was ended on the 12th March, 13 days before the expected end date and the Cornell campus was closed the previous week. The early end date had no effect on CBETA commissioning as project funding for CBETA had ended by this point.

Progress on the CBETA inverse Compton scattering source (ICS) was affected as in person discussions between Kirsten Deitrick (my Cornell mentor and co-author of the paper) and I about the design of the bypass lattice and writing of the paper were disrupted and ended abruptly.

Introduction

Energy recovery Linacs (ERLs) are ideal drivers of inverse Compton scattering sources (ICS) due to the combination of linac quality beams and high repetition rate, allowing production of a tunable high-flux, narrowband scattered photon beam. The pioneering demonstration of multi-pass energy recovery in a superconducting RF (SRF) linac with FFAG return loop at the Cornell University Brookhaven National Laboratory Energy Recovery Linac Test Accelerator (CBETA) reveals a route to high energy electron beams for ERL driven ICS production of X-rays and γ-rays.

Due to a $E_\gamma \propto 4\gamma^2$ scattered photon energy E_γ dependence, where γ is the Lorentz factor, ICS is the prime candidate for production of high energy photons above photon energies available at conventional X-ray production facilities such as Free Electron Lasers (FEL)($E_\gamma < 25$ keV [1]) and the largest synchrotrons ($E_\gamma < 500$ keV). Therefore, inverse Compton scattering sources are also the eminent method for high-flux production of γ-rays ($E_\gamma \sim 1$ MeV), which could support applications like nuclear resonance fluorescence (NRF) and nuclear photonics. ICS sources can be optimised to produce photons in smaller natural bandwidth than synchrotron radiation, alleviating the need for monochromators which inherently deplete the flux of the source.

Experience gained this year from participating in CBETA commissioning and designing an X-ray ICS utilizing CBETA will ultimately motivate design choices and optimisations for an inverse Compton source operating on the posited Daresbury Industrial Accelerator for Nuclear Physics Applications (DIANA) ERL. The design values for the CBETA ICS are 9.28×10^8 ph/s in a 0.5% bandwidth up to a maximum photon energy of 401.4 keV. In comparison, the DIANA γ-ray source will be capable of producing 10^{11} ph/s in a 0.5% bandwidth with scattered photon energies in the 1-20 MeV range, competitive with the flagship ELI-NP-GBS [2] linac based inverse Compton scattering source.

Summary of 2nd Year Work

CBETA Commissioning

A Long Term Attachment (LTA) at Cornell University facillitated participation in the multi-pass commissioning of CBETA. Experience was gained in tuning the splitter and recombiners of the first two passes of the ERL. CBETA commissioning also provided training in setting up the injector and main linac cryomodules, and running simple accelerator control and measurement scripts such as dispersion and orbit correction.

Commissioning experience exposed difficulties in operating accelerators in general, such as energy drifts, and obstacles unique to ERLs, like the requirement for precise control of path length correction. As well as this, understanding challenges unique to CBETA commissioning including the effect of stray fields and challenges posed by common transport, which involves accelerating and decelerating beams in a shared beamline, could contribute to plans for future ERLs.

As a secondary operator, both a control and measurement script were devised. This acted as an introduction to accelerator control and measurement systems. Understanding the complexities of measurement and control of an ERL is informative toward designing sources which are easier to operate than CBETA and may avoid it's pitfalls. For example, multi-turn ERL's require substantial forethought when writing measurement scripts as altering the machine can have a knock-on effect on both previous and future passes; common transport such as the FFAG return loop and splitter lines of CBETA further exacerbate this difficulty.

The control script was a pyEPICS based degauss all magnets function designed to mitigate hysteresis in CBETA's electromangnets. The degauss all magnets script varies the current of the main accelerator magnets (excluding the injector and merger magnets) and permanent magnet corrector coils as prescribed by a degaussing procedure used for the LCLS injector [3]. The degaussing script performed well and was subsequently used within other control and measurement scripts.

A chromaticity script was constructed to measure the chromaticity per cell, in both planes, of sections of the accelerator, such as the FFAG recirculation line and splitter/recombiner sections, for all 4 turns. Chromaticity measurement was accomplished by recursively applying a modified version of an existing script used to measure tune in sections of the machine whilst incrementing the beam energy through adjustment of cavity 1 voltage (the cavity traversed last by an accelerated beam). Unfortunately, this script was only tested on the last day of operation; due to energy drift in the linac only measurements up to the second turn produced usable data when this was compared to the expected tune produced from fieldmaps.

With CBETA's FFAG common transport, which involves multiple energy accelerating and decelerating beams in a shared beamline, optics are coupled for each energy and for both the accelerating and decelerating passes. This causes numerous difficulties in tuning the accelerator optics as adjusting an accelerating pass via the splitter simultaneously adjusts a decelerating pass and any adjustment of the FFAG alters every pass. Therefore, tuning can only really be accomplished with the splitter lines on accelerating passes up to the highest energy 150 MeV pass – decelerating passes are not tunable directly. Measurement and control are also complicated by common transport, for example whilst performing a quadrupole scan to measure a response matrix for an orbit correction, the variation in quadrupole strength affects the optics of the previous pass via stray fields. Practical insight into operating a multi-pass common transport ERL is valuable for design decisions regarding optics in ERL's and their applications.

CBETA Inverse Compton Source

An inverse Compton source has been designed to produce high-energy X-rays from the 4th pass (150 MeV) electron beam, the highest nominal beam energy of the CBETA ERL. The CBETA ICS would be capable of producing X-rays up to 400 keV, close to the photon energy limit of large synchrotrons. The CBETA ICS is competitive in terms of flux with large scale synchrotron facilities such as Spring-8 in this scattered photon energy domain producing $\sim 10^9$ ph/s within a 0.5% bandwidth. Output parameters of the CBETA ICS highlight the photon energy interface where conventional X-ray production facilities are succeeded by inverse Compton scattering sources.

Design of a bypass lattice offset vertically from the 4-pass configuraton of CBETA is required due to spatial requirements of an ICS interaction point. The bypass diverts the electron beam after the 4th accerating pass of the linac via a vertical dogleg in the splitter and focuses the beam at the ICS interaction point through a flexible final focus system ($\beta^* =$ 1-12 cm demonstrated, as set by optimisation). After the interaction, the bypass performs path length correction of the electron beam with a maximum range of a single RF wavelength either side of the nominal solution – more than sufficient for energy recovery and also corrects the R_{56} of the electron beam. The bypass maintains the same Twiss parameter and zero dispersion match into the 1st decelerating pass of the linac; recovering the matching conditions of the standard 4th pass.

Lattice design challenges of an ERL ICS such as space considerations for an interaction point, extraction of an X-ray beam and optics matching considerations have become clear. Whilst avoided in the current 150MeV bypass configuration, implementing an ICS or an ICS bypass into a common transport beamline such as the lower passes of CBETA would prove challenging optically as constraints on both the accelerating and decelerating beams would have to be satisfied and the IP would need to be designed to accommodate both beams. Common transport is a potential obstacle to ICS facilities utilizing each nominal energy of a common transport multi-turn ERL.

Electron beam parameters were set for the ICS operational mode based on the design parameters of CBETA. Laser pulse and re-circulation cavity parameters were chosen based on the most recent demonstration of an ERL based inverse Compton scattering source at cERL [4] and the state of the art demonstration of an optical re-circulation cavity [5]. Parameters such as the beta function at the IP and collimation angles were optimised through the bandwidth tuning algorithm detailed in the next section. Output spectral parameters have been calculated analytically using the source parameters. A journal paper specifying the CBETA ICS design is in progress, with the majority of the source design and calculation aspects finalised.

ICS Bandwidth Tuning

Small bandwidth ($< 1\%$) scattered photon beams are advantageous because a smaller energy spread of the photon beam increases precision of measurements; some experiments like parametric down conversion [6] and Non-resonant Inelastic X-ray Scattering (NIXS) require small bandwdith. Small bandwidth photon beams can also avoid the use of monochromators and simplify the X-ray/γ-ray optics required for experiments. High flux is also necessary to observe rare processes and improve

the counting statistics of experiments. A trade-off detailed here can be performed to maximise the flux of an ICS in a selected bandwidth.

A method has been devised, based on the scaling laws by N. Ranjan et al [7], to optimise an inverse Compton source by the β function at the interaction point β^* and the collimation angle θ_{col} so that the ICS satisfies a user determined bandwidth requirement. Used in conjunction with a method by L. Serafini et al [8] to calculate the collimated flux in a given collimation angle, a bandwidth tuning algorithm has been created to optimise an ICS to the user defined bandwidth and calculate the maximal flux in this bandwidth whilst returning the β^* and θ_{col} parameters for this case.

The bandwidth tuning algorithm has been used to produce tuning curves for the bandwidth and flux in selected bandwidth for both the CBETA ICS and the posited DIANA ERL ICS. It has been discovered that the minimum bandwidth of an inverse Compton source is dependent on the energy spread of the electron beam and that in the Thomson regime, where the photon – electron interaction can be modelled as an elastic collision i.e. the recoil of the electron is negligible, the tuning curves are independent of beam energy.

The method of calculating the maximal collimated flux in a selected bandwidth has been benchmarked against simulations by Illya Drebot for the same purpose. The calculation was based on a high intensity laser, single-shot version of the proposed 340 MeV pass of the DIANA ICS and calculated collimated flux in a 0.5% bandwidth. The methods differ as Illya's method uses Conglomérat d'ABEL et d'Interactions Non-Linéaires (CAIN) [9], a Monte Carlo simulation code, to calculate the collimated flux whereas my method is purely analytical. The optimisation methods also appear to differ although I am not aware of the exact details of Illya's bandwidth optimisation. The calculation of flux in a 0.5% bandwidth differed by $\sim 6\%$ between methods, which is considered to be a good agreement as both the optimisation and the collimated flux calculation differed.

Future Work and Thesis Plan

Analytical Spectrum

It would be advantageous to study the effect of emittance, energy spread and other laser pulse and electron beam parameters on ICS output by observing their effect on the scattered photon spectrum. The ICS spectrum can be produced analytically [10], analytically using a tracked particle bunch in the Improved Code for Compton Scattering (ICCS) [7] or via Monte Carlo simulation in CAIN. These spectrum production methods should be compared against each other to validate their use in high repetition rate inverse Compton sources as these are typically applied to the high intensity laser and low repetition rate linac driven scenario. Spectra could be used to validate the analytical calculations of the output source parameters and investigations into the effect of accelerator and laser parameters on the spectra could inspire further optimisation methods.

A spectrum for the CBETA ICS has been produced via CAIN, however CAIN suffers from an inability to properly simulate recirculated ICS and poor statistics in the tails of the distribution or at very narrow apertures [7]. Collimation is not included in CAIN spectra produced so far, which should be rectified.

Work is ongoing into replicating C. Sun et al's [10] model which will be benchmarked against the results from C. Sun's paper and Krafft et al's paper [7], which simulates an identical scenario.

DIANA inverse Compton Scattering Source

Design investigations into a γ-ray ICS for the proposed DIANA multi-pass ERL will continue. Preliminary calculations have been performed for an ICS in the 1st Year of the PhD, which can be extended and improved using experience from the CBETA ICS design, for example the optimisation code developed this year can be applied and calculations can be extended to include collimation.

Spectra could also be produced for the DIANA ICS once the analytical spectrum code is operational. Spectra can be produced for each nominal energy for a variety of laser pulse and electron beam parameters which would enable investigations into possible designs for the ICS and some optimisation of parameters such as bunch length, emittance and energy spread which could inform design choices for the ERL.

Thesis Plan

A provisional timescale for the write-up of the thesis is shown in Fig. 1. The chapter headings for the thesis are:

- Introduction
- Theory of Photon Production by Inverse Compton Scattering
- CBETA Inverse Compton Source Design
- DIANA Inverse Compton Source Design
- CBETA Multi-pass Commissioning

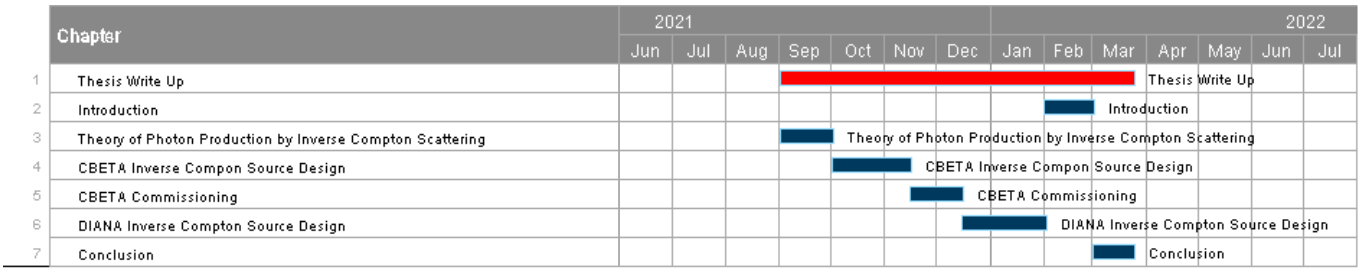

Figure 1: Timescale for the write-up of the thesis.

- Conclusions

References

[1] Evgeny A Schneidmiller and Mikhail V Yurkov. Photon Beam Properties at the European XFEL (December 2010 revision). Technical report, Deutsches Elektronen-Synchrotron (DESY), 2011.

[2] O Adriani, S Albergo, D Alesini, M Anania, D Angal-Kalinin, P Antici, A Bacci, R Bedogni, M Bellaveglia, C Biscari, et al. Technical Design Report EurogammaS Proposal for the ELI-NP Gamma Beam System. *arXiv preprint arXiv:1407.3669*, 2014.

[3] Achim W Weidemann. A Degaussing Procedure for the QG01 Quadrupole Magnet of the LCLS Injector Beamline. Technical report, SLAC National Accelerator Lab., Menlo Park, CA (United States), 2006.

[4] T Akagi, A Kosuge, S Araki, R Hajima, Y Honda, T Miyajima, M Mori, R Nagai, N Nakamura, M Shimada, et al. Narrow-band Photon Beam via Laser Compton Scattering in an Energy Recovery Linac. *Physical Review Accelerators and Beams*, 19(11):114701, 2016.

[5] Henning Carstens, N Lilienfein, Simon Holzberger, C Jocher, T Eidam, J Limpert, A Tünnermann, J Weitenberg, Dylan C Yost, A Alghamdi, et al. Megawatt-Scale Average-Power Ultrashort Pulses in an Enhancement Cavity. *Optics letters*, 39(9):2595–2598, 2014.

[6] P Eisenberger and SL McCall. X-ray Parametric Conversion. *Physical Review Letters*, 26(12):684, 1971.

[7] Nalin Ranjan, B Terzić, GA Krafft, Vittoria Petrillo, Illya Drebot, and L Serafini. Simulation of Inverse Compton Scattering and its Implications on the Scattered Linewidth. *Physical Review Accelerators and Beams*, 21(3):030701, 2018.

[8] C Curatolo, I Drebot, V Petrillo, and L Serafini. Analytical Description of Photon Beam Phase Spaces in Inverse Compton Scattering Sources. *Physical Review Accelerators and Beams*, 20(8):080701, 2017.

[9] P Chen, G Horton-Smith, T Ohgaki, AW Weidemann, and K Yokoya. Cain: Conglomerat d'abel et d'interactions non-lineaires. *Nuclear Instruments and Methods in Physics Research Section A: Accelerators, Spectrometers, Detectors and Associated Equipment*, 355(1):107–110, 1995.

[10] C Sun, J Li, G Rusev, AP Tonchev, and YK Wu. Energy and Energy Spread Measurements of an Electron Beam by Compton Scattering Method. *Physical Review Special Topics-Accelerators and Beams*, 12(6):062801, 2009.

Intense Monochromatic Photons Above 100 keV From An Inverse Compton Source at the Cornell-BNL ERL Test Accelerator

Kirsten Deitrick, Georg Hoffstaetter, Vaclac Kostroun, and Carl Franck
Cornell University, USA

Peter Williams and Bruno D. Muratori
STFC Daresbury Laboratory and Cockcroft Institute, UK

Hywel Owen and Joe Crone
The University of Manchester and Cockcroft Institute, UK

Balša Terzić
Old Dominion University, USA
(Dated: June 30, 2020)

Quasi-monochromatic X-rays are difficult to produce above 100 keV, but have a number of potential uses that include fluorescence identification and quantification of transuranic nuclides. Inverse Compton scattering (ICS) of an intense 1064 nm laser can generate photon energies extending into the MeV regime from modest electron energies. Here we predict the expected ICS flux from the operating 42–150 MeV CBETA multi-turn energy-recovery linac using incident laser repetition rates up to 325 MHz. Collimated fluxes around 10^9 photons per second in a 0.5% bandwidth are expected using demonstrated CBETA bunch properties, with scattered photon energies extending beyond 400 keV for electron energies of 150 MeV. The ICS flux exceeds that attainable from storage ring sources of synchrotron radiation, in a compact accelerator system. We foresee that future energy-recovery linacs may generate MeV photon energies with properties not attainable using other methods, enabling wide applications in nuclear physics and applications that today utilise undulator radiation.

I. INTRODUCTION

Intense sources of high-energy photons above 1 keV can be obtained in the laboratory in one of four practical ways: discrete line gamma sources from radioactive decay, bremsstrahlung of electrons within a solid target, synchrotron radiation (SR), and inverse Compton scattering (ICS). Such sources are today the mainstay of many areas of scientific study; for example, GeV-scale electron storage ring production of narrowband undulator X-rays over 1 to 100 keV has broad uses across many topics in diffraction and spectroscopy, whilst broadband MeV-scale bremsstrahlung from lower-energy electrons (in the c.10 MeV regime) finds applications in imaging and nuclear physics, particularly when applied to the identification and quantification of nuclear materials.

Although bremsstrahlung can be used to generate photon energies above 50 keV they are not ideal. Important techniques using high-energy photons are x-ray absorption spectroscopy (XAS), x-ray fluorescence (XRF), and nuclear resonance fluorescence (NRF) which for samples with high atomic number Z have numerous applications in nuclear physics, industry, and nuclear security. For example, a high-Z nucleus such as uranium ($Z = 92$) has Kα_2 and Kα_1 energies of 94.7 keV and 98.4 keV respectively (K edge energy 115.6 keV) – photons of higher energies are needed to probe transuranic species. Similarly, NRF can be used to discriminate with precision the quantities of transuranic isotopes in large samples (such as spent nuclear fuel canisters) using photons in the 1 to 3 MeV range (^{235}U detection needs 1.733 MeV photons). Bremmsstrahlung sources intrinsically generate a large quantity of unused photons at lower energies that cause a number of operating and instrumental issues; ideally, a monochromatic (or quasi-monochromatic) source is wanted. Electron storage rings at the higher practicable stored bunch energies around 6-8 GeV (such as the national facilities ESRF, APS and SPRING-8) can generate intense, monochromatic photons up to 100 keV in the first harmonic of their undulators. However, these sources are hardly compact (the storage rings are around 1 km in circumference), and their output does not readily extend to the MeV scale.

ICS using the common 1064 nm incident wavelength ($E_{\text{laser}=1.16}$ eV photon energy) in the head-on geometry gives backscattered photons with energy

$$E_\gamma = 4\gamma^2 E_{\text{laser}} \tag{1}$$

for electrons with Lorentz factor $\gamma = E_e/m_e c^2$. Electrons with energy

Here we describe the advantages offered by an energy recovery linac (ERL) driven ICS light source as an intense source of high energy photons, and provide an example of such a source based on the recently-commissioned multi-turn ERL utilizing superconducting radiofrequency (SRF) cavities: CBETA - the Cornell-BNL ERL Test Accelerator. We show below that the bunch parameters demonstrated can provide a flux of monochromatic X-rays that can extend up to 400 keV, providing a flux not readily attainable in other ways.

Something about Compton formula and MeV photons. Statement about storage sources and their capabilities at 100 keV

Basic head-on formula, laser wavelength/energy -¿ typical scattered energies.

In the future, the highest-power accelerators will likely be limited to storage rings and ERLs – the power cost of linacs will simply be too great. CBETA is an example of energy efficient accelerator design, combining the energy efficient concepts of energy recovery and permanent magnet transport, and serves as an example for design concepts and considerations necessary for these future high-power accelerators [**?**].

II. THE CBETA ACCELERATOR

A. Motivation for an Energy Recovery Linac

In the early days of high energy accelerators, two main categories existed: linear and circular. Today, linacs and storage rings are commonplace in the accelerator community. As a generalization, linacs are typically capable of producing higher-quality beams than storage rings. However, this comes with a lower energy efficiency than a storage ring; a typical storage ring current would be impossible in a linac - the radiofrequency (RF) power cost would be prohibitively expensive.

ERLs are a type of machine that combines the best of both types of accelerators; they can typically deliver higher quality beams than those in storage rings, with greater energy efficiency than a linac. In a typical one-turn ERL, a low energy beam is injected into a string of SRF cavities which accelerate the beam, the beam is then transported back to the entrance of the cavity string, where the beam is then decelerated, before being transported to the beam dump; an example layout and details of the beam path are shown in Fig. 1. The power "recovered" by the cavities in the process of decelerating the beam is then used to accelerate the next bunch without additional RF power; this allows for the beam power in the ERL to exceed the available RF power. As the beam parameters necessary for scientific research call for higher current and higher quality beams, ERLs are the accelerators best suited to meet this demand. Multi-turn ERLs, which accelerate the electron beam multiple times before decelerating the beam, have the benefit of being able to reach higher energies without additional cost, power requirements, or floor space [1].

B. The Cornell-BNL ERL Test Accelerator

The Cornell-BNL ERL Test Accelerator, CBETA, is the first successful demonstration of an SRF multi-turn ERL [2**?**]; additionally, it features a non-scaling Fixed-Field Alternating-gradient (FFA) arc constructed out of permanent (Halbach-type) combined-function magnets, which transport four beam energies (42, 78, 114, and 150 MeV) simultaneously in a common transport beam pipe. CBETA consists of a 6 MeV injector, single main linac cryomodule (MLC), splitter/recombiner sections (SX and RX), FFA arc (FA, TA, ZX, TB, FB), and beam stop; the layout of the four-turn configuration, is shown in Fig. 1.

Parameter	Quantity	Units
Energy	42, 78, 114, and 150	MeV
RF frequency	1.3	GHz
Bunch charge	$\leq$2	nC
Repetition rate	1.3/N (some integer)	GHz
Maximum current	100 (one-turn), 40 (four-turn)	mA

TABLE I: Key design parameters of CBETA.

CBETA may be configured to operate using one to four turns, with the corresponding top energies of each configuration given by 42, 78, 114, and 150 MeV, respectively; the design parameters are given in Table I. For a configuration of Y turns, the beam completes $2Y$ passes through the MLC, and $2Y-1$ passes through the FFA arc. The FFA arc can be divided into five sections: the arc sections (FA, FB) consist of FFA arc cells; the straight section (ZX) consists of FFA straight cells; and the transition sections (TA, TB) serve to match the beam between the arc and straight sections.

In the SX and RX sections, each beam energy passes through a different splitter/recombiner; this gives control of the Twiss parameters, horizontal dispersion and its derivative, R_{56}, and orbit; path length is varied by moving the stages. The SX/RX lines are numbered one to four (S1, S2, etc) corresponding to increasing beam energy, with the lowest-energy splitter line (S1 or R1) on the inside, and successive higher-energy lines further out. Each splitter line simultaneous transports two beams – an accelerated pass and a decelerated pass – apart from at the highest-energy pass. Consequently, the design optics of the accelerating and decelerating passes in the splitter lines are inherently coupled [2].

III. COMPARISON OF INVERSE COMPTON SCATTERING AND OTHER RADIATION SOURCES

A. Inverse Compton Scattering

Following their original description by Feenberg and Primakoff [3], sources based on inverse Compton scattering (ICS) – the process of scattering a photon off of a relativistic electron – have emerged as a promising way to generate tuneable, monochromatic photons across output energies from tens of keV up to even GeV scale [4–6]. The energy of scattered photons, taking into account electron

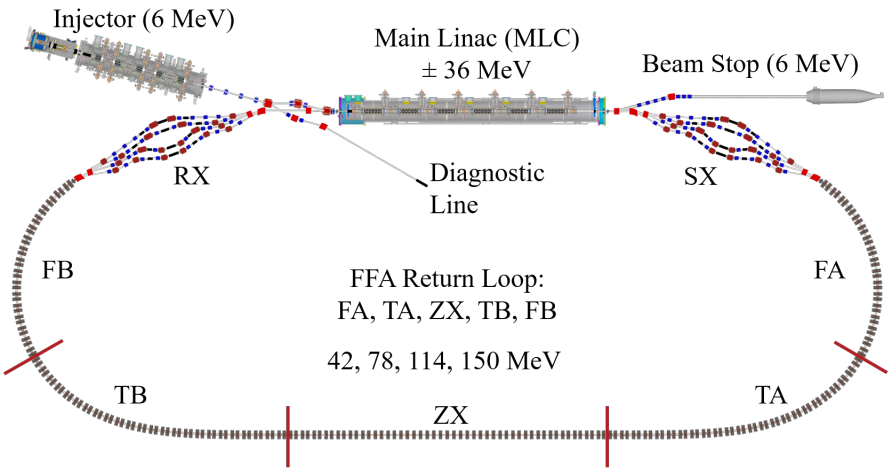

FIG. 1: Overview of the operating CBETA accelerator; a single FFA arc transports multiple passes.

recoil, is given by

$$E_\gamma = \frac{E_{\text{laser}}\,(1-\beta\cos\phi')}{1-\beta\cos\theta+(1-\cos\theta')E_{\text{laser}}/E_e} \tag{2}$$

where E_{laser} is the energy of the laser, β is the typical relativistic factor of v_z/c, θ represents the angle between the electron beam and the scattered x-rays, ϕ' represents the angle between the incident electron and incident photon, $\theta' = \phi' - \theta$ is the angle between the incident and scattered photons, $\phi = \pi - \phi'$ is the crossing angle, and E_e is the energy of the electron beam; the geometry of the interaction point (IP) can be seen in Fig. 2 [7, 8].

The highest energy x-rays are produced in a head-on collision between the electron and incident laser beams ($\phi' = \pi$), with the highest energy x-rays scattered in the same direction that the electron beam travels ($\theta = 0$). This is referred to as the Compton edge, and no higher energy radiation is emitted. Taking the electron recoil into account, the maximum energy of the scattered photons is given by

$$E_\gamma^{\max} = \frac{4\gamma^2 E_{\text{laser}}}{1+X},$$

where $X = 4\gamma E_{\text{laser}}/mc^2$ is the electron recoil parameter [9]. In the Thomson regime, electron recoil is negligible (i.e. $X \ll 1$), and the maximum energy becomes

$$E_\gamma^{\max} = 4\gamma^2 E_{\text{laser}}.$$

In this regime, the scattering interaction can be viewed as an elastic collision. Electron recoil becomes significant when both γ and E_{laser} are large, and in this situation

$$E_\gamma \to E_e$$

(where $E_e = \gamma mc^2$ is the total electron energy); the scattered photon energy cannot have more energy than the electron had. A practical example is the proposed collision of 12 keV FEL photons with 7 GeV electrons within a storage ring ($X \sim 1000$), where the scattered photon energy becomes essentially also 7 GeV [10].

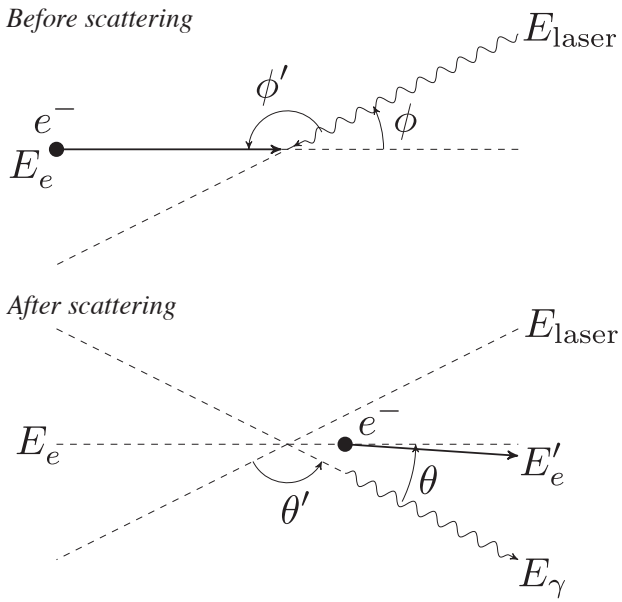

FIG. 2: Geometry of scattering at the inverse Compton Scattering interaction point; follows Fig. 1 from Sun et al. [8].

Compton scattering can be treated as analogous to undulator radiation; in that vein, the undulator K-parameter is similar to the laser field strength parameter a_0 for Compton scattering , which is given by

$$a_0 = \frac{eE\lambda_{\text{laser}}}{2\pi mc^2} \tag{3}$$

where e is the electron charge, E the transverse electric field of the laser, $\lambda_{\rm laser}$ is the wavelength of the incident laser, and mc^2 is the rest energy of the electron. In the linear regime, $a_0 \ll 1$, and all formulae are constructed in that regime [7].

The total number of scattered photons N_γ per collision as a function of the collision angle is given by

$$N_\gamma = \sigma_c \frac{N_e N_{\rm laser} \cos(\phi/2)}{2\pi\sigma_y \sqrt{\sigma_x^2 \cos^2(\phi/2) + \sigma_z^2 \sin^2(\phi/2)}} \quad (4)$$

where σ_c is the Compton scattering cross-section, $\sigma_{r,i}^2 = \sigma_{{\rm electron},i}^2 + \sigma_{{\rm laser},i}^2 (i = x, y, z)$ is the convoluted spot size of the electron and laser beam at the IP in each plane, and the number of electrons and photons at the IP respectively N_e and $N_{\rm laser}$. The exact Compton cross-section from QED is

$$\sigma_c = \sigma_T \frac{3}{4X} \left[\left(1 - \frac{4}{X} - \frac{8}{X} \right) \log(1+X) \right. \quad (5)$$

$$\left. + \frac{1}{2} + \frac{8}{X} - \frac{1}{2(1+X)^2} \right], \quad (6)$$

which reduces to

$$\sigma_c \simeq \sigma_T (1 - X) \quad (7)$$

for small values of X; here $\sigma_T = 6.65 \times 10^{-29}$ m^2 is the Thomson cross section [11]. For $\lambda_{laser} = 1064$ nm and typical $\gamma \sim 10^3$ we have $X \sim 10^{-2}$, and thus $\sigma_c \simeq \sigma_T$ to the percent level.

Assuming a plane wave approximation of the incident laser, the number of scattered photons within a 0.1% bandwidth at the Compton edge is $N_{0.1\%} = 1.5 \times 10^{-3} N_\gamma$. Consequently, the rate of photons (flux) into this bandwidth is $\mathcal{F}_{0.1\%} = 1.5 \times 10^{-3} \dot{N}_\gamma$; for repetitive sources, $\dot{N}_\gamma = f N_\gamma$, where f is the repetition rate [7]. In the non-diffraction limited case with the laser spot significantly larger than the electron beam spot at the IP, the average brilliance of the scattered x-rays (given in conventional units, i.e. mm^{-2}mrad^{-2} s^{-1} per 0.1%bw) is given by

$$\mathcal{B}_{\rm avg} \approx \frac{\mathcal{F}_{0.1\%}}{4\pi^2\epsilon^2} = \frac{\gamma^2 \mathcal{F}_{0.1\%}}{4\pi^2 \epsilon_N^2}, \quad (8)$$

where ϵ is the transverse emittance of the electron beam at the IP; ϵ_N is the normalised transverse emittance, where we assume a round beam. For a more detailed explanation, refer to [12].

The peak brilliance of the source is calculated via an analytical formula by Hartemann et al. [13]

$$\mathcal{B}_{\rm peak} = 10^{-15} \frac{4\gamma^2}{\pi^2 \epsilon_N^2} \frac{N_e N_L}{\Delta\tau} \frac{r_0^2}{\sigma_{\rm laser}^2} \exp\left\{ \frac{\chi - 1}{2\chi \Delta u_\perp^2} \left[2 + \frac{\delta\omega^2 + \delta\gamma^2\chi^2}{2\chi(\chi-1)\Delta u_\perp^2} \right] \right\} \times \left[1 - \Phi\left\{ \frac{\chi - 1}{\sqrt{\delta\omega^2 + \delta\gamma^2\chi^2}} \left[1 + \frac{\delta\omega^2 + \delta\gamma^2\chi^2}{2\chi(\chi-1)\Delta u_\perp^2} \right] \right\} \right] \mathbb{F}(\eta, \mu), \quad (9)$$

where r_0 is the classical electron radius, $\Delta u_\perp = \epsilon_N / \sigma_{\rm electron}$ is the perpendicular velocity spread, with $\sigma_{\rm electron}$ the spot size of the electron beam at the IP (assuming a circular beam spot), $\Delta\tau$ is the electron bunch duration, $\delta\omega$ is the relative frequency spread of the laser, $\delta\gamma$ is the relative energy spread of the electron beam; the 10^{-15} factor originates as a unit conversion from SI to mm^{-2}mrad^{-2}s^{-1} per 0.1% bw. The normalised Doppler up-shifted frequency, χ is given by

$$\chi = \frac{\omega_x}{4\gamma^2 \omega_0}, \quad (10)$$

where ω_x and ω_0 are the angular frequency of the scattered and incident radiation, $\Phi(x)$ is the error function,

$$\Phi(x) = \frac{2}{\sqrt{\pi}} \int_0^x e^{-t^2} dt. \quad (11)$$

The overlap function $\mathbb{F}(\eta, \mu)$ is given by

$$\mathbb{F}(\eta, \mu) = \frac{\eta e^{1/\eta^2} [1 - \Phi(1/\eta)] - \mu e^{1/\mu^2} [1 - \Phi(1/\mu)]}{\eta^2 - \mu^2}, \quad (12)$$

where $\eta = c\Delta t / 2\sqrt{2}\beta^*$ is the normalised inverse β function, Δt is the laser pulse duration, β^* the β-function at the IP, and $\mu = c\Delta t / 2\sqrt{2} z_R$ is the normalised inverse Rayleigh length for Rayleigh length $z_R = \pi\sigma_{\rm laser}^2 / \lambda$.

The spectral density of the output spectra is calculated here as

$$\mathcal{S} = \frac{\mathcal{F}}{E_\gamma}, \quad (13)$$

where $\mathcal{F} = f N_\gamma$ is the total uncollimated flux and E_γ is the energy of the scattered photon (Eq. 2).

Using the bandwidth arising from the scaling laws by N. Ranjan et al. [9], the bandwidth of the scattered radiation can be expressed by

$$\frac{\Delta E_\gamma}{E_\gamma} = \sqrt{\left(\frac{\sigma_\theta}{E_\theta}\right)^2 + \left(\frac{\sigma_e}{E_e}\right)^2 + \left(\frac{\sigma_L}{E_L}\right)^2 + \left(\frac{\sigma_\epsilon}{E_\epsilon}\right)^2}, \quad (14)$$

$$\frac{\sigma_\theta}{E_\theta} = \frac{1}{\sqrt{12}} \frac{\Psi^2}{1+X+\Psi^2/2}, \tag{15}$$

$$\frac{\sigma_e}{E_e} = \frac{2+X}{1+X+\Psi^2} \frac{\Delta E_e}{E_e}, \tag{16}$$

$$\frac{\sigma_L}{E_L} = \frac{1+\Psi^2}{1+X+\Psi^2} \frac{\Delta E_{\text{laser}}}{E_{\text{laser}}}, \tag{17}$$

$$\frac{\sigma_\epsilon}{E_\epsilon} = \frac{2\gamma\epsilon^N}{\beta^*}. \tag{18}$$

where $\Psi = \gamma\theta_{\text{col}}$ is the acceptance angle, θ_{col} is the collimation angle, X is the electron recoil parameter, $\Delta E_e/E_e = \delta\gamma$ is the energy spread of the electron beam, $\Delta E_{\text{laser}}/E_{\text{laser}} = \delta\omega$ is the laser energy spread, β^* is the β-function at the IP, and ϵ^N is the normalized emittance of the electron beam at the IP.

This formula allows for the contributions to the bandwidth of the scattered radiation to be separated into individual contributions from the collimation system (Eq. 15), electron beam energy spread (Eq. 16), laser energy spread (Eq. 17), and electron beam emittance (Eq. 18).

B. ICS Accelerator and Parameter Considerations

This consistently talks about X-rays but everything mentioned is general, should X-rays be replaced with scattered photons? Based on the previous formulae, relationships emerge between electron beam properties and the parameters of the scattered x-rays; the following assumes fixed laser properties and electron beam energy. The x-ray flux increases with the increasing bunch charge and repetition rate and with decreasing electron spot size and bunch length. The average brilliance increases with increasing flux and decreasing transverse emittance; the peak brilliance has the same relationships and increases with decreasing bunch length. The bandwidth decreases with decreasing energy spread of the electron beam, the ratio of ϵ^N/β^*, and collimation angle, Ψ.

In designing an ICS source, a number of trade-offs are necessary, due to the conflicting demands of electron beam dynamics and hardware limitations. The ideal scattering laser is typically produced by a high power optical cavity (∼100 kW or greater), which limits the repetition rate of the interaction to a few hundred MHz – as the repetition rate increases, the optical cavity path length decreases, which amplifies the engineering challenges of the laser cavity such as sensitivity to misalignment errors, mirror heating, etc.

Taking these relationships into consideration, the electron beam should be generated by a high repetition rate source, with a high brightness and low energy spread. For high-flux a smaller electron beam spot size at the IP is needed, while a larger spot is necessary for a low-bandwidth configuration. However, it is preferable that an ICS source is capable of adjusting the optics at the IP between these two operational modes, i.e., a dual-mode ICS source.

A high-brightness, low-energy-spread electron beam for a dual-mode ICS is more likely to be produced by a linac or an ERL than a storage ring. Additionally, while a storage ring is capable of handling greater beam currents, operating the accelerator at a repetition rate greater than the repetition rate of the optical cavity does not produce additional x-rays. Increasing the bunch charge only maintains average brilliance if the electron beam emittance growth is proportional to the square root of the increase in bunch charge - otherwise, average brilliance decreases.

For high energy x-rays, the operating power cost is significantly reduced in ERL compared to a linac; a multi-turn ERL has the added benefit of requiring less floor space and fewer SRF cavities. Consequently, a multi-turn ERL with a high brightness, low energy spread electron beam at a high repetition rate is an ideal accelerator for a dual-mode ICS source; CBETA is such an accelerator and in section IV, details will be given about the anticipated operation of CBETA as an ICS source.

C. Comparison with Other Radiation Sources

The four principle methods of photon production in the 100 keV to 10 MeV range are subject to quite different limitations, and we briefly summarise them.

So-called line sources of gamma rays are obtained from samples of long-lived gamma-ray emitters such as ^{137}Cs and ^{60}Co. They have been widely used in radiotherapy, imaging and sterilisation and give the narrowest bandwidths, but are difficult to handle, emit isotropically, and cannot be tuned to different photon energies. Bremsstrahlung sources produce mainly longer-wavelength photons and relatively fewer extending up to the Duane-Hunt limit $\lambda = hc/E_k$; however, they can readily generate MeV photons from small-footprint systems.

Synchrotron radiation sources such as undulators can provide intense, tuneable radiation. The characteristic critical photon energy is

$$\epsilon_c = \frac{3}{2} \frac{\hbar c \gamma^3}{\rho}, \tag{19}$$

which may be written as ϵ_c [keV] $\simeq 0.665 E^2 B$ (for E give in GeV and B in tesla; this sets the scale for attainable photon energy. n GeV and B is the magnetic flux density of the dipole magnet given in Tesla. The highest-energy 3rd-generation SR source today is SPRING-8 with $E =$ 8 GeV and $B \simeq 0.68$ T to obtain a critical energy $\epsilon_c \simeq$ 29 keV for its broadband incoherent SR production; it

is unlikely that a storage ring above 8 GeV will be built since rings such as SPRING-8 already have a physical circumference exceeding 1000 m. The undulator output limit from a storage ring can be illustrated by setting the undulator K-parameter to be $K \sim 1$ and an undulator period $\lambda_u \sim 1$ cm. This gives a magnetic field limit of

$$B_0 = \frac{m_e c}{e} \frac{2\pi}{\lambda_u} K \sim 1\text{T}. \tag{20}$$

The minimum undulator wavelength $K = 0$ possible (in the first harmonic of emission) is

$$\lambda_{\min} = \frac{\lambda}{2\gamma^2} \simeq 0.2\text{Å} \tag{21}$$

at 8 GeV ($\gamma \simeq 15{,}700$), which corresponds to a photon energy of 60 keV. Operating undulators at SPRING-8 obtain photon energies

SR sources such as undulators and free-electron lasers can provide intense, tuneable monochromatic radiation, but it is costly to obtain high photon energies. The critical photon energy for a bending radius ρ is

$$\epsilon_c = \frac{3}{2} \frac{\hbar c \gamma^3}{\rho}, \tag{22}$$

which may be written as

$$\epsilon_c \text{ [keV]} \simeq 0.665 E^2 B \tag{23}$$

where E is the electron beam energy given in GeV and B is the magnetic flux density of the dipole magnet given in Tesla. The highest-energy 3rd-generation SR source today is SPRING-8 with $E = 8$ GeV and $B \simeq 0.68$ T to obtain a critical energy $\epsilon_c \simeq 29$ keV for its broadband incoherent SR production; it is unlikely that a storage ring above 8 GeV will be built since rings such as SPRING-8 already have a physical circumference exceeding 1000 m. The undulator output limit from a storage ring can be illustrated by setting the undulator K-parameter to be $K \sim 1$ and an undulator period $\lambda_u \sim 1$ cm. This gives a magnetic field limit of

$$B_0 = \frac{m_e c}{e} \frac{2\pi}{\lambda_u} K \sim 1\text{T}. \tag{24}$$

The minimum undulator wavelength $K = 0$ possible (in the first harmonic of emission) is

$$\lambda_{\min} = \frac{\lambda}{2\gamma^2} \simeq 0.2\text{Å} \tag{25}$$

at 8 GeV ($\gamma \simeq 15{,}700$), which corresponds to a photon energy of 60 keV. This limit on undulator output is seen in practice, and there are very few undulator beamlines worldwide that deliver photons above 50 keV; the spectral brightness also falls dramatically.

Compared to traditional light sources such as synchrotrons, Compton sources produce x-rays in a significantly narrower bandwidth, which is necessary for many applications. While narrow bandwidth x-rays are available at SR sources, this is achieved by monochromators; SR sources are inherently wide band. However, monochromators start to lose their efficacy as the x-ray energy increases. Consequently, for a higher energy x-ray beam, the source must inherently be narrow band for applications requiring a narrow bandwidth. X-ray free electron lasers (XFELs), while also producing narrow-bandwidth x-rays, typically have a higher user cost and generally have a maximum x-ray energy on the order of 10 keV, which prevents them from functioning as a high-energy x-ray source. Consequently, Compton sources can complement existing light sources by producing high-intensity, high-energy x-rays, which are not found at existing sources, and with the option to operate in either high flux and narrow bandwidth modes. The average and peak brilliance of various light sources as a function of x-ray energy are shown in FIGURE, with the properties of a Compton source at CBETA and the more typical range of other Compton sources indicated.

IV. INVERSE COMPTON PRODUCTION AT CBETA

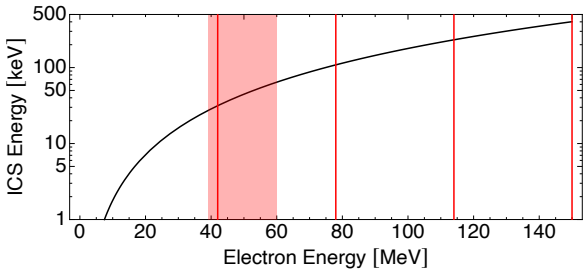

FIG. 3: An ICS source generating photons from each of the four CBETA ERL passes delivers the scattered energies indicated here, assuming an incident laser wavelength of 1064 nm. CBETA has demonstrated tuning of a single pass energy from 39 to 60 MeV, which indicates the ICS tuning that an ERL might deliver at other energies.

A. Electron and Laser Beam Properties

Based on the desired properties of an electron beam given previously (high brightness, low energy spread) and the capabilities of CBETA, with the key design parameters given in Table I, the desired electron beam parameters at the IP are given in Table II. The table is divided into three sections – parameters which are constant between the high flux and narrow bandwidth modes are given at the top, while the beam size, β^*, and collimation angle for the high flux and narrow bandwidth modes are given at the middle and bottom, respectively.

While the design of CBETA allows for a maximum current nearly four times greater than the desired electron beam, the coherent synchrotron radiation (CSR) effects on the beam necessitate a lower bunch charge [14]; the repetition rate cannot be increased due to the hardware limitations of the optical cavity providing the laser.

As the focus of this paper is not on optical cavity design, laser parameters based on existing [11] and state-of-the-art systems [15] have been proposed and are given in Table III. In the event that the repetition rate needs to be reduced by a factor of two due to optical cavity limitations, it may be feasible to double the pulse energy of the laser and keep the x-ray parameters of the resulting beam unchanged.

Fig. 3 seems to not be referenced in the text at all. Would it be worth having a statement in this section saying that CBETA has been demonstrated over a specific range of beam energies which correspond to the possible tuning range shown in Fig. 3? Mention what may be possible in terms of beam energy range in the higher passes? below does that but is fairly shit

As part of the single pass commissioning of CBETA the FFAG was tested with electron beams in an energy range from 39 to 60 MeV. Therefore the CBETA ICS could potentially be operated within this range. This would allow tuning of X-ray energy in the range 27.2 to 64.5 keV from the adjustment of the first pass configuration. Fig. 4 shows the possible scattered photon energies from the electron beam energy tuning range of all passes.

B. Interaction Bypass Lattice

In order to utilize CBETA as an inverse Compton scattering source, a bypass line is required due to the stringent space restrictions of the existing FFA return loop, which leaves no space for the final focus and laser recirculation cavity required for an ICS interaction point. The scattered X-rays from the ICS must also be produced in a different plane to the existing accelerator as the X-rays must be safely extracted from the footprint of the ERL since there is no space for an experimental hutch within the CBETA hall. The layout of such a bypass line is shown in Fig. 4. The bypass is configured for 150 MeV 4-pass operation but could be developed to operate with all nominal energies.The bypass was designed and optimised using the Bmad [16] and Tao [17] lattice codes. ***is “lattice codes“ the correct description?***

The bypass design diverts the 150 MeV electron beam after the fourth linac pass in the corresponding S4 splitter line; the electron beam then re-enters the existing layout in the R4 line. The bypass replaces the FFA return loop, S4 from the 4th dipole onward and R4 up to the 4th dipole. The bypass will be located above the existing permanent magnet arc as the FFA arc is still used to transport the lower energy (42, 78, and 114 MeV) beams before and after the bypass.

A system of vertical doglegs, replacing sections of the S4 and R4 lines, are required to provide a 30 cm vertical elevation of the bypass line relative to the plane of the FFA return loop in order to avoid the existing accelerator. Bypass arc sections replace the existing FFA arc sections (FA, FB). Following the first arc, there is a horizontal dogleg used to close horizontal dispersion before the interaction region and offset the bypass from existing infrastructure.

At the interaction region (IR) the beam is again offset upward locally by a further 20 cm to a 50 cm total offset above the FFA reference orbit using a set of vertical doglegs, the IR doglegs. The further vertical offset is imposed so the x-rays are produced in a different plane to both the bypass line and FFA return loop. A flexible focusing section within the set of IR doglegs is used to focus to the required beam waist. The final focus section has been shown to focus to both $\beta^* = 1$ cm, for the high-flux case and $\beta^* = 12.6$ cm for the 0.5% bandwidth case from Table II. The final focus section is constructed from 7 quadrupoles with the laser re-circulation cavity placed between the 4th and 5th quadrupole. This scheme allows the x-rays to be extracted via the first dipole of the second IR dogleg, minimizing the number of magnets requiring modification for x-ray extraction.

Within the straight section of the bypass following the IR, a variable path length chicane is implemented based on the focusing chicane in the modular path length correction design by H. Owen et al [18]. The 4 dipole focusing chicane uses two swinging arms with a variable length bellow between the interior dipoles. Each arm has a focusing system of three quadrupoles. The dipoles are initially set to minimise the R_{56} of the lattice. The focusing system in the arms, which is located in a dispersive area, can then be used to provide further R_{56} correction. Unlike in the modular path length correction design [18], the CBETA bypass does not use a non-focusing chicane as the additional R_{56} correction this provides is not required as the arcs within the bypass have the required flexibility for R_{56} correction. $R_{56} = 0$, the condition required for the 150 MeV pass in the standard CBETA return loop has been replicated for the high flux and 0.5% cases of the bypass.

Path length adjustment is possible by varying the strength of the focusing chicane dipoles concurrently and adjusting the variable length bellow accordingly. By increasing the strength of the dipoles the path length can be increased, and by decreasing the strength of the dipoles the path length is decreased. It has been demonstrated that the path length of the bypass lattice can be altered by $\pm\lambda_{RF}$, an RF wavelength either direction of the nominal solution. Path length adjustment of a single RF wavelength is adequate for energy recovery of the electron beam in an ERL.

Plots of the dispersion and β functions throughout the bypass line in the 0.5% bandwidth are shown in Figs. 5 and 6. Tuning of the optics of the bypass was limited by the compact nature of CBETA, conditions required for

TABLE II: Electron beam parameters at the IP. Where one value is given, it applies to all four beam energies; where four values are given, each corresponds to one of the four energies. Parameters which are constant between the high flux and narrow bandwidth modes are given at the top, while the beam size, β^*, and collimation angle for the high flux and narrow bandwidth modes are given at the middle and bottom, respectively.

Parameter	Quantity				Unit
Beam energy	42	78	114	150	MeV
Repetition rate	325				MHz
Bunch charge	32				pC
Transverse normalized *rms* emittance	0.3				mm-mrad
rms bunch length	1.0 (3.33)				mm (ps)
Relative energy spread	5.0×10^{-4}				
	High flux				
β^* at the IP	1				cm
Beam spot size	6.04	4.43	3.67	3.20	µm
Collimation angle	something				mrad
	0.5% bandwidth				
β^* at the IP	3.5	6.6	9.6	12.6	cm
Beam spot size	11.3	8.3	6.9	6.0	µm
Collimation angle	1.551	0.836	0.572	0.435	mrad

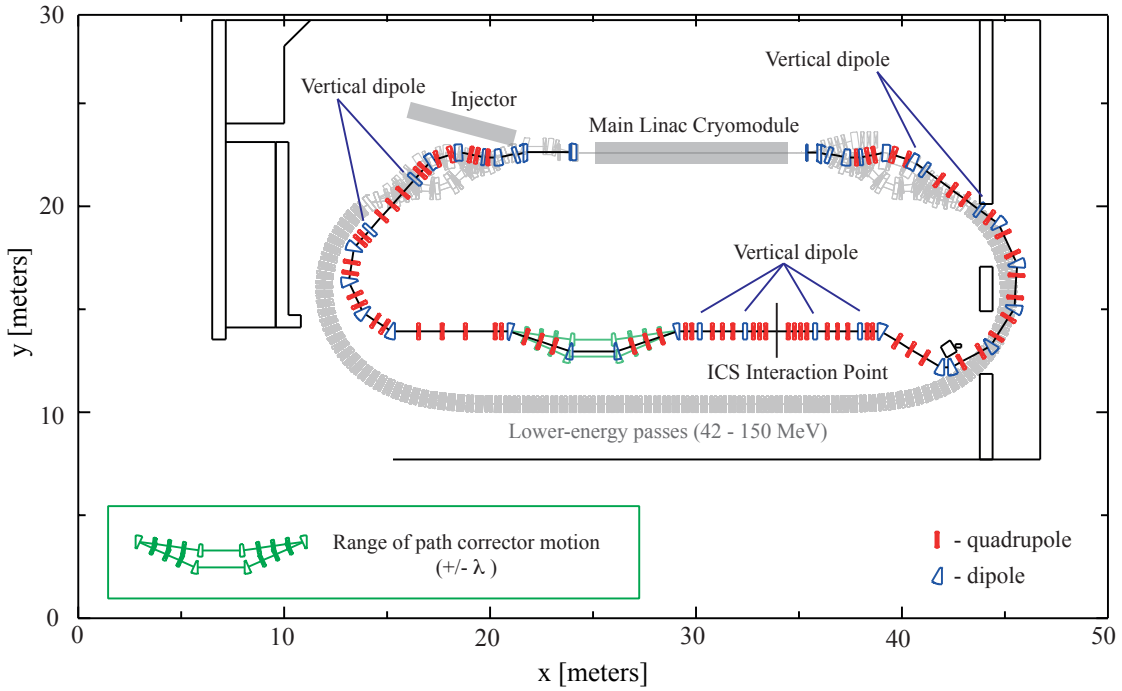

FIG. 4: Layout of the ICS bypass in CBETA.

energy recovery of the interacted beam, and the necessity for the bypass to be constructed above the existing FFA return loop.

C. Bandwidth Tuning

The bandwidth of the CBETA ICS is tuneable and will be selected on the basis of user requirements. Bandwidth selection is possible through the tuning of the beta function of the electron beam at the interaction point, β^*, and the collimation angle, $\theta_{\rm col}$, of the scattered X-ray radiation. The former is controlled through adjustment of the final focus quadrupoles in the IR and the latter via a variable collimation system.

Typically the dominant terms in the unoptimised bandwidth of an inverse Compton source (Eq. 14) are the collimation term (Eq. 15) and the emittance term

TABLE III: Laser beam parameters at the IP.

Parameter	Quantity	Unit
Wavelength	1064	nm
Pulse energy	62	µJ
Repetition rate	325	MHz
Spot size at the IP	25	µm
Crossing angle	5°	
Pulse length	10	ps
Relative energy spread	6.57×10^{-4}	

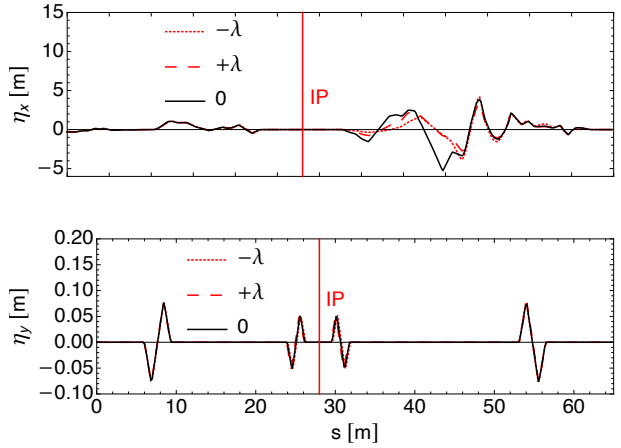

FIG. 5: Dispersion functions in the ICS bypass line for the 0.5% bandwidth case. The ICS interaction point (IP) is indicated.

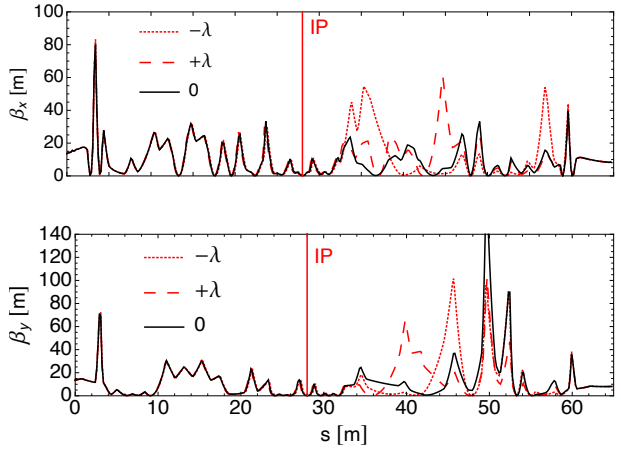

FIG. 6: Twiss functions in the ICS bypass line. The ICS interaction point (IP) is indicated.

(Eq. 18). The free parameter of the collimation term is $\theta_{\rm col}$, which can be adjusted through the aperture size of a collimator and the distance it is placed from the interaction point. Adjustable collimators have been designed for the ELI-NP-GBS γ-ray inverse Compton scattering source [19]; a similar design would be implemented here.

The emittance term is dependent on both the normalised transverse emittance ϵ^N and β^*. It is convenient to change the beta function at the interaction point instead of the normalised emittance, which is dependent on the injector and collective effects throughout the bypass lattice, as the beam waist is controlled via the final focus. Therefore, with a small collimator aperture and small beam waist it is possible to reduce the contribution of the collimation and emittance terms until they are negligible and the beam energy spread term (Eq. 16) is dominant, assuming the contribution of the laser energy spread term (Eq. 17) is negligible which is typical of conventional lasers. This effectively places a lower limit on the bandwidth of a conventional laser inverse Compton source, which is governed by the energy spread of the electron beam $\Delta E_e/E_e$ as

$$\left(\frac{\Delta E_\gamma}{E_\gamma}\right)^{\rm min} \approx 2\frac{\Delta E_e}{E_e} \tag{26}$$

Consequently, any bandwidth above this limit can be achieved by an inverse Compton source through the tuning of the collimation angle and β^* so that a desired bandwidth, $\Delta E_\gamma/E_\gamma$, is achieved. Since the collimation and emittance terms are typically dominant, all other terms can be excluded and the solutions are bounded by

$$\frac{\Delta E_\gamma}{E_\gamma} > \sqrt{\left(\frac{\Delta\sigma_{\theta_{\rm col}}}{E_{\theta_{\rm col}}}\right)^2 + \left(\frac{\Delta\sigma_\epsilon}{E_\epsilon}\right)^2}. \tag{27}$$

This results in myriad combinations of β^* and $\theta_{\rm col}$ which satisfy a bandwidth requirement greater than the lower limit (Eq. 26).

However, these solutions all produce varying collimated flux as the flux through the collimator is dependent on both the beam waist (which is proportional to β^*) and the collimation angle. The solution that is most preferable maximizes the x-ray flux, so the collimated flux needs to be calculated for each solution. The collimated flux $\mathcal{F}_\Psi$ of each solution is calculated based on a method valid for small angle collimation ($\gamma\theta_{\rm col} < 1$) by L. Serafini et al [20] and modified for these purposes becomes

$$\mathcal{F}_\Psi = \mathcal{F} \times \frac{\left(1+\sqrt[3]{X}\Psi^2/3\right)\Psi^2}{\left[1+(1+X/2)\,\Psi^2\right](1+\Psi^2)}, \tag{28}$$

where $\mathcal{F}$ is the total uncollimated flux, $\Psi = \gamma\theta_{\rm col}$, and X is the recoil parameter. The solution giving the maximal flux is selected.

In practice, it is not feasible to create an algorithm that performs this method on all solutions. Instead, an array of collimation angles $\theta_{\rm col}$ from 0 to $1/\gamma$ is used ($\gamma\theta_{\rm col} < 1$), and for a given bandwidth value, the corresponding β^* is calculated using

$$\beta^* = \frac{2\gamma\epsilon^N}{\sqrt{\left(\frac{\Delta E_\gamma}{E_\gamma}\right)^2 - \left[\left(\frac{\sigma_{\theta_{\rm col}}}{E_{\theta_{\rm col}}}\right)^2 + \left(\frac{\sigma_e}{E_e}\right)^2 + \left(\frac{\sigma_{\rm laser}}{E_{\rm laser}}\right)^2\right]}}, \tag{29}$$

which is a rearrangement of (Eq. 14). The solutions based on this array of collimation angles are plotted in β^* - $\theta_{\rm col}$ space for the case of 0 - 1% bandwidth for the CBETA ICS in Fig. 7.

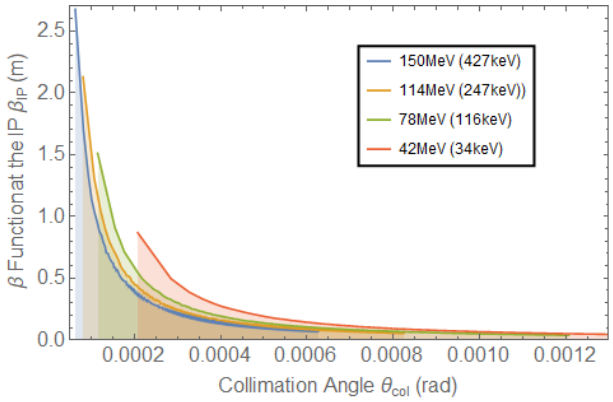

FIG. 7: Tuning curves of the β^* against $\theta_{\rm col}$ for each of the nominal CBETA electron beam energies satisfying the maximal flux across the 0 - 1% bandwidth range. Minimised bandwidth solutions in this range have large β functions at the IP and small collimation angles $\theta_{\rm col}$, the maximal bandwidth solutions have small β functions and larger collimation angles $\theta_{\rm col}$.

The collimated flux $\mathcal{F}_\Psi$ is calculated for each combination produced via this method. The maximal collimated flux is selected and the combination of β^* and $\theta_{\rm col}$ corresponding to this solution is returned. This process can be applied to the case of a target bandwidth to determine $\theta_{\rm col}$, β^*, and collimated flux in the selected bandwidth.

In addition, applying this method to a continuum of bandwidths allows us to map the possible operational settings of our inverse Compton scattering source and plot tuning curves, such as the plot of the collimated flux against the bandwidth for a 0 - 1% bandwidth range in Fig. 8.

D. X-ray Production and Spectra

The parameters of the spectrum of scattered radiation from the source have been calculated analytically from the formulae in Section III A. The results of these calculations are shown in Table IV. This table also includes results for the collimated flux in the 0.5% case which have been produced using the analytical method outlined in Section IV C. The collimated flux in the high flux case at 150 MeV has been produced through the integration of the spectral plot in Fig FIGURE.

Plots of the spectra of the scattered radiation from the CBETA ICS have been produced using the analytical energy spectra code ICCS [9, 21] which uses the parameters in Tables II and III, and the distribution of a Gaussian bunch tracked through the Bmad bypass lattice, as outlined in Section IV, using Tao. Fig. FIGURE shows the

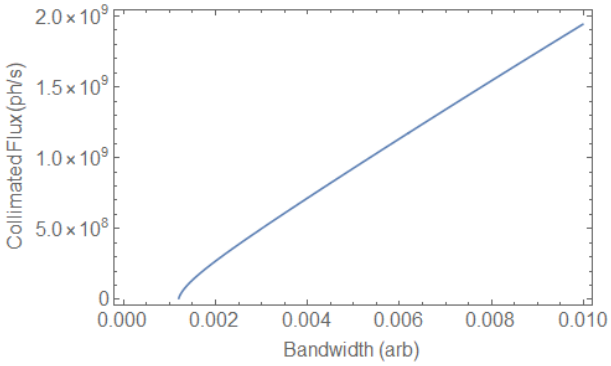

FIG. 8: Collimated flux against bandwidth tuning curve for 0-1% bandwidth range, produced via tuning β^* the beta function at the IP and $\theta_{\rm col}$ the collimation angle. The tuning curve is independent of beam energy in the Thomson regime, hence the tuning curve applies to all of the nominal energies of CBETA. The tuning curve ends at the minimum bandwidth of the source $\sim 0.1\%$.

energy spectra for the high flux case and Fig. FIGURE shows the energy spectra for the 0.5% bandwidth case.

V. DISCUSSION

A. Applications

Complete Work in progress! Needs plenty of work

The CBETA ICS is a high-flux, small bandwidth quasi-monochromatic ICS source of X-rays, producing high peak energy photons in the uncharted 100's keV range. As a consequence this opens up a parameter space for X-ray applications previously attainable only through the largest synchrotrons, with substantial X-ray optics. meaning monochromators and the like

Important applications of such a source are X-Ray absorption spectroscopy (XAS) and X-Ray fluorescence (XRF), [22] (P. Willmott, Chapter 6, "Spectroscopic Techniques" in "An Introduction to Synchrotron Radiation: Techniques and Applications," (Wiley, which for samples with high atomic number Z have numerous applications in nuclear physics, industry [23] *** Example of XRF of fuel rod***, and nuclear security. For example, a high-Z nucleus such as uranium ($Z = 92$) has Kα_2 and Kα_1 energies of 94.7 keV and 98.4 keV respectively (K edge energy 115.6 keV) – and photons of higher energies are needed to probe transuranic species.

Using high energy XRF one can illuminate the sample to be analyzed with the collimated source, there is no need to monochromate. Energy sensitive X-ray fluorescence detection would be provided by a solid state detector coupled to a pulse height analyzer. For the analysis of a fission reactor's fuel rods, the K alpha and beta lines for uranium at 98 and 111 keV as well as the plutonium lines at 104 and 117 keV could be probed. Quantitative

TABLE IV: Anticipated x-ray parameters for each of the four electron beam energies. Parameters common among both modes are given in the top section of the table, while other parameters for the high flux and narrow bandwidth cases are given in the middle and lower sections, respectively.

	Electron Beam Energy (MeV)				
Parameter	42	78	114	150	Unit
X-ray peak energy	31.5	108.7	232.0	401.4	keV
Uncollimated flux	6.31×10^{10}	6.39×10^{10}	6.42×10^{10}	6.43×10^{10}	ph/s
Spectral density	2.00×10^{6}	5.88×10^{5}	2.77×10^{5}	1.60×10^{5}	ph/s eV
Average brilliance	1.80×10^{11}	6.28×10^{11}	1.35×10^{12}	2.34×10^{12}	ph/s mm^2 mrad^2 0.1% bw
High flux					
Peak brilliance	2.73×10^{15}	9.90×10^{15}	2.16×10^{16}	3.77×10^{16}	ph/s mm^2 mrad^2 0.1% bw
0.5% bandwidth					
Collimated flux	9.29×10^{8}	9.29×10^{8}	9.29×10^{8}	9.28×10^{8}	ph/s 0.5%bw

assays would be performed by means of a low-Z reference scatterer to ascertain the spectral content of the broadband incident beam through elastic and Compton scattering into the same detector. The fluorescence efficiency of the detection scheme is then provided by the known photoabsorption cross sections of the elements of interest vs incident energy.

A third ready application exploits the high flux and high energy by the source: energy dispersive X-ray difraction (EDXRDD) for the identification of constituents of a polycrystalline/powdered sample. Thanks to the high flux, this would allow for rapid identification of the minerals in a mined ore sample. One can inspect thick specimens thanks to the high energy of the source. In EDXRD [24](B. Kämpfe F. Luczak B. Michel, "Energy Dispersive X-Ray Diffraction," Part. Part. Syst. Charact. 22 391 (2005)) one applies the unmonochroamted peak to a specimen of the material of interest and checks for diffracted photons with an energy sensitive solid state detector. From the energy we deduce the wavelength and applying the Bragg relation we find the combination of Miller indices and lattice spacing of the reflecting crystalline planes. Checking for many such reflections for a particular mineral provides constituent identification. The intensity of these Bragg peaks provides the relative abundances of the various mineral components.

Turning to more ambitious but equally exciting applications, in contrast with the other applications, significant beamline infrastructure would be required in these cases. In the first, we propose to perform Nonresonant Inelastic X-ray Scattering (NIXS) in order to examine the dynamic electronic response of quantum materials throughout the periodic chart. The high incident energy and high flux provided by our source allows us to test exciting materials such as transition metal oxides, which are test bed for theories such as the Mott-Hubbard model as they provide fresh insight into the candidates for useful applications such as high temperature superconductors. (reference issacs and eisensberger) ***not enough info to find this reference*** The energy resolution requirements are severe: 1 eV out of 100 keV. This would require the development of a high energy X-ray monochromator and analyzer optics, most likely through synthetic multilayers in order to provide an optimal match for our beam optics. In our implementation of the NIXS technique the analyzers are arrayed at a range of scattering angles to provide a comprehensive set of momentum transfers. The pass energy of the analyzers is fixed while the incident energy is scanned to provide variable energy tarnsfers with a double crystal monochromator configuration. (Reference schulke, LERIX at APS) ***not enough info to find this reference***

In our second ambitious application for the current accelerator, a mixing crystal would be employed to generate entangled photon pairs via parametric down conversion (PDC). Here the efficiency is boosted by working at high input energy since the intensity of the vacuum fluctuations present at the mixer's input goes as the fourth power of the operating energy. [25](P. Eisenberger and S.L. McCall, X-Ray Parametric Conversion, Phys. Rev. Letts. v. 26, 684 (1971)). Besides the accomplishment of achieving PDC at about a factor of five (check) higher energy than has been hitherto achieved, it will provide exciting applications: e.g. twin microscopy which promises enhanced visibility through quantum ghost imaging of otherwise inaccessible specimens and twin ellipsometry for the careful examination of surface structures.

The final ambitious application, nuclear resonance fluorescence (NRF), would require a fourth pass ***This needs re-looked, we already have 4 passes and an extra pass would take us to 186 MeV which is 620 keV photons, NRF is useful in the MeV range right? extra pass + 2nd harmonic Ti:Sa ($\lambda = 532$ nm) laser gets us to 1.24 MeV.*** in order to boost the incident electron beam energy into the realm in which we our Compton back scattered beam would produce MeV gamma rays. These in turn would be used to excite nuclear levels identifying them with a energy sensitive solid state detector, achieving the nuclear sister spectroscopy to the atomic fluorescence spectroscopy mentioned in our first application. Such spectroscopy would be very useful in assaying nuclear materials e.g. in spent fission fuel. (give reference to Val and Bruce Dunham's presentation and the one Peter recently provided: Geddes 2017 "Impact

of Monoenergetic Photon Sources on Nonproliferation Applications")[26] ***Geddes report***

VI. CONCLUSION

ACKNOWLEDGEMENTS

This work was supported in part by xxx under xxx This work was supported in part by the Science and Technology Facilities Council under Grant Nos. ST/G008248/1 and ST/S505523/1. We would like to thank Geoff Krafft, for useful discussions.

ANSWERING CORRECTIONS/QUESTIONS

$a_0 \ll 1$ is the linear regime; if I was feeling cruel, I would suggest that you calculate what a_0 is $a_0 = 4.09 \times 10^{-5}$, it is more a statement that our theory section is only valid in the linear regime - for example no ponderomotive broadening term in the bandwidth etc.

Is Doubling pulse energy for a halved rep rate possible?

Doubling the pulse energy of our laser gives us ~ 0.124 mJ, at a 162 MHz rep rate, so $P_{\text{cav}} = 20.1$ kW. My calculations of the power per unit area on the mirrors for the double pulse energy, half rep rate case yields $1.91{\times}10^9$ W m^{-2} for the worst case scenario (square cavity) and assuming Gaussian optics. Based on a mirror heating limit $P/A = 10^{10} - 10^{11}$ W m^{-2} (coating damage of mirrors) suggested by F. Zomer this is feasible.

The 'state of the art' [15] for a cavity is $P_{\text{cav}} = 670$ kW with a 10 ps pulse length, 1040 nm wavelength and 250 MHz repetition rate. This results in a pulse energy $E_{pulse} = 2.68$ mJ.

Doubling our pulse energy should be possible, this cavity was demonstrated but I'm unclear about it's feasibility as the paper makes it clear this is at the damage threshold of the mirrors. It seems that a mJ level, 100's MHz cavity is possible but difficult, this hasn't been demonstrated/designed as part of an ICS yet - hence my skepticism to quote higher numbers.

Happy to show this calculation if there is interest.

WHY DOES BILL GRAVES HAVE DIFFERENT BRILLIANCES FOR DIFFERENT BANDWIDTHS?

I'm still working on this, the paper is long and taking a long time to understand. It gives a lot of different parameters but never parameters for the bandwidth cases.

The source size (vertically 1.8 μm to 1.9 μm, horizontally 2.4 μm to 2.5 μm) and opening angles (1 mrad increase horizontally and vertically) increased from the 0.1% to 5% case. This means a smaller β^* and larger collimation angle for the 5% case but I suspect more changes that aren't explicitly stated occur.

The flux increases from the 0.1% case (2×10^{10} ph/s) to the 5% case (5×10^{11} ph/s), this is stated in units of photons per second, we would expect this result as β^* is slightly smaller but a factor of 25x larger seems a lot. It is unclear whether this is raw flux or flux in a particular bandwidth, though I'm guessing it is the latter. w_0 the laser waist is 2x larger than the beam size at the IP, so small mm scale changes in β^* would have negligible affect on flux.

However both the average and peak brilliance decreases for the 5% case which seems really odd to me. β^* is smaller so 'raw' flux for this case is larger The average brightness (6) is calculated similarly to ours, no peak brilliance calculation is shown. (6) shows no reason why this would vary with bandwidth.

The source parameters must have some variation in parameters between cases to explain the factor of 3.5 reduction in average brilliance and factor of 3.3 reduction in peak brilliance. Opening angle alone should not have an affect as the 0.1% bandwidth part of the spectrum is undisturbed by this in both cases.

In conclusion: I don't know.

[1] L. Merminga, D. R. Douglas, and G. A. Krafft, High-current energy-recovering electron linacs, Annual Review of Nuclear and Particle Science **53**, 387 (2003), https://doi.org/10.1146/annurev.nucl.53.041002.110456.

[2] G. Hoffstaetter, D. Trbojevic, and C. Mayes, CBETA design report, Tech. Rep. (Brookhaven National Laboratory (BNL), Upton, NY (United States), 2017).

[3] E. Feenbergand H. Primakoff, Interaction of cosmic-ray primaries with sunlight and starlight, Phys. Rev. **73**, 449 (1948).

[4] R. H. Milburn, Electron scattering by an intense polarized photon field, Phys. Rev. Lett. **10**, 75 (1963).

[5] F. Arutyunianand V. Tumanian, The compton effect on relativistic electrons and the possibility of obtaining high energy beams, Physics Letters **4**, 176 (1963).

[6] C. Bemporad, R. H. Milburn, N. Tanaka, and M. Fotino, High-energy photons from compton scattering of light on 6.0-gev electrons, Phys. Rev. **138**, B1546 (1965).

[7] G. A. Krafftand G. Priebe, Compton sources of electromagnetic radiation, Reviews of Accelerator Science and Technology **03**, 147 (2010), https://doi.org/10.1142/S1793626810000440.

[8] C. Sun, J. Li, G. Rusev, A. Tonchev, and Y. Wu, Energy and energy spread measurements of an electron beam by compton scattering method, Physical Review Special Topics-Accelerators and Beams **12**, 062801 (2009).

[9] N. Ranjan, B. Terzić, G. Krafft, V. Petrillo, I. Drebot, and L. Serafini, Simulation of inverse compton scattering and its implications on the scattered linewidth, Physical Review Accelerators and Beams **21**, 030701 (2018).

[10] H. R. Weller, M. W. Ahmed, H. Gao, W. Tornow, Y. K. Wu, M. Gai, and R. Miskimen, Research opportunities at the upgraded hiγs facility, Progress in Particle and Nuclear Physics **62**, 257 (2009).

[11] T. Akagi, A. Kosuge, S. Araki, R. Hajima, Y. Honda, T. Miyajima, M. Mori, R. Nagai, N. Nakamura, M. Shimada, T. Shizuma, N. Terunuma, and J. Urakawa, Narrow-band photon beam via laser compton scattering in an energy recovery linac, Phys. Rev. Accel. Beams **19**, 114701 (2016).

[12] K. E. Deitrick, G. A. Krafft, B. Terzić, and J. R. Delayen, High-brilliance, high-flux compact inverse compton light source, Phys. Rev. Accel. Beams **21**, 080703 (2018).

[13] F. Hartemann, W. Brown, D. Gibson, S. Anderson, A. Tremaine, P. Springer, A. J. Wootton, E. Hartouni, and C. Barty, High-energy scaling of compton scattering light sources, Physical Review Special Topics-Accelerators and Beams **8**, 100702 (2005).

[14] W. Louand G. H. Hoffstaetter, Coherent synchrotron radiation wake expressions with two bending magnets and simulation results for a multiturn energy-recovery linac, Phys. Rev. Accel. Beams **23**, 054404 (2020).

[15] H. Carstens, N. Lilienfein, S. Holzberger, C. Jocher, T. Eidam, J. Limpert, A. Tünnermann, J. Weitenberg, D. C. Yost, A. Alghamdi, et al., Megawatt-scale average-power ultrashort pulses in an enhancement cavity, Optics letters **39**, 2595 (2014).

[16] D. Sagan, The Bmad Manual, Available at: `https://www.classe.cornell.edu/bmad/manual.html` ((2019)).

[17] D. Sagan, The Tao Manual, Available at: `https://www.classe.cornell.edu/bmad/tao.html` ((2019)).

[18] H. L. Owenand P. H. Williams, A modular path length corrector for recirculating linacs, Nuclear Instruments and Methods in Physics Research Section A: Accelerators, Spectrometers, Detectors and Associated Equipment **662**, 12 (2012).

[19] G. Paternò, P. Cardarelli, M. Marziani, E. Bagli, F. Evangelisti, M. Andreotti, M. Gambaccini, V. Petrillo, I. Drebot, A. Bacci, et al., A collimation system for elinp gamma beam system–design and simulation of performance, Nuclear Instruments and Methods in Physics Research Section B: Beam Interactions with Materials and Atoms **402**, 349 (2017).

[20] C. Curatolo, I. Drebot, V. Petrillo, and L. Serafini, Analytical description of photon beam phase spaces in inverse compton scattering sources, Phys. Rev. Accel. Beams **20**, 080701 (2017).

[21] G. Krafft, E. Johnson, K. Deitrick, B. Terzić, R. Kelmar, T. Hodges, W. Melnitchouk, and J. Delayen, Laser pulsing in linear compton scattering, Physical Review Accelerators and Beams **19**, 121302 (2016).

[22] P. Willmott, An introduction to synchrotron radiation: techniques ar (John Wiley & Sons, 2019).

[23] G. J. Havrilla, V. Lopez, K. McIntosh, W. Elam, and D. Robinson, Feasibility of uranium detection through container walls using ultrahigh-energy x-ray fluorescence, Microscopy Today **23**, 30 (2015).

[24] B. Kämpfe, F. Luczak, and B. Michel, Energy dispersive x-ray diffraction, Particle & Particle Systems Characterization **22**, 391 (2005).

[25] P. Eisenbergerand S. McCall, X-ray parametric conversion, Physical Review Letters **26**, 684 (1971).

[26] C. A. Miller, B. Ludewigt, B. J. Quiter, S. Pozzi, and C. G. Geddes, Assessing impact of monoenergetic photon sources on nonproliferation applications, Transactions **117**, 1029 (2017).